

UDC 528.481

IMPACT OF DATA STRUCTURE TYPES AND SPATIAL RESOLUTION ON LANDSLIDE VOLUMETRIC CHANGE MEASUREMENTS

Ján ŠAŠAK ¹, Ján KAŇUK ^{1, 3✉}, Miloš RUSNÁK ², Jozef ŠUPINSKÝ ¹

¹*Institute of Geography, Faculty of Science, Pavol Jozef Šafárik University in Košice, Košice, Slovakia*

²*Department of Physical Geography, Geomorphology and Natural Hazards, Institute of Geography, Slovak Academy of Science, Bratislava, Slovakia*

³*PHOTOMAP, s.r.o., Poludníková 3/1453, 04012 Košice, Slovakia*

Article History:

- received 19 December 2023
- accepted 03 December 2024

Abstract. Terrain is a dynamic component of the landscape, subject to rapid changes, particularly in scenarios such as landslides. This study investigates how the spatial resolution and data structure of digital terrain models (DTMs) influence the estimation of landslide volume changes. We selected a landslide formed by the undercutting action of the Belá River in Slovakia as our research site. Our findings indicate that raster data structures, across various spatial resolutions, generally yield more consistent volume estimates compared to 3D mesh data structures. Nonetheless, at higher spatial resolutions (0.1 m and 0.25 m), the 3D mesh data structure demonstrates superior capability in capturing detailed terrain features, resulting in more precise volume estimations of the landslide.

Keywords: landslide, laser scanning, volume change estimation, 2D raster model, 3D mesh model, spatial resolution.

✉ Corresponding author. E-mail: jan.kanuk@photomap.sk

1. Introduction

Remote sensing (RS) technologies are designed for topographic mapping and enable the parameterization of the intricate geometric structures of various terrain features. RS technologies offer an unparalleled level of spatial resolution (LoSR) and can capture data over arbitrary time intervals (Casagli et al., 2017; Zhong et al., 2019; Lissak et al., 2020; Alvarez-Vanhard et al., 2021). The quality of the data is crucial when studying terrain changes, especially given the need for repeated measurements to ensure efficient data collection. At present, the predominant methods for monitoring landslides are RS techniques that employ laser scanning (Abellán et al., 2011; Pellicani et al., 2019; Jiang et al., 2021; Marotta et al., 2021; Kermarrec et al., 2022) and photogrammetry (James & Robson, 2012; Scaioni et al., 2015; Antoine et al., 2020; Devoto et al., 2020; Kyriou et al., 2021; Mineo et al., 2022). These geospatial data collection methods yield a discrete point field of elevations, commonly known as a point cloud, which characterizes exceptional spatial resolution and accuracy (Guerra-Hernández et al., 2018; Tian et al., 2019; Dong et al., 2020). After further processing, this data can be used to generate various surface types such as digital terrain models (DTM)

(Zhang et al., 2018; Agüera-Vega et al., 2020), digital elevation models (DEM) (Peterson et al., 2019; Mishra et al., 2020), canopy height models (CHM) (Tian et al., 2019; Zhang et al., 2021), tree surface models (Münzinger et al., 2022; Nguyen et al., 2022), ice surfaces (Alfredsen et al., 2018; Huang et al., 2019), and building surfaces (Wang & Kim, 2019; Chen et al., 2022).

Terrain refers to the geometric characteristics of a specific landscape surface, particularly its elevation, slope, aspect, and other morphometric parameters. In digital contexts, terrain is defined as a two-dimensional continuous field of elevations that represent terrain shapes. This representation exists within a 3D space using raster models (Šašak et al., 2019; Dolejš et al., 2020). Vector models, such as irregular triangulated networks (TIN) (Ai et al., 2019), or mesh structures (Gallay et al., 2015; Harding et al., 2021), are also used. In certain applications, a discontinuous yet densely populated point cloud (e.g., with more than 1000 points/m²) can be employed as an alternative representation (Šupinský et al., 2019; Kuželka et al., 2020). A common research objective related to terrain is examining changes over time, such as the volumetric alterations in rock material and soil, whose surfaces exemplify the terrain. It is related, for example, to the dynamics of

landslides and rocks (Kyriou et al., 2021; Mazzanti et al., 2021; Meng et al., 2021; Stumvoll et al., 2021), erosion of coastal cliffs (Devoto et al., 2020; Caputo et al., 2018; De Sanjosé Blasco et al., 2020; Roulland et al., 2022), by the transformation of the river bed (Calle et al., 2018; Nourbakhshbeidokhti et al., 2019; Akay et al., 2022), erosion of river banks (Duró et al., 2018; Rice et al., 2021), and other related phenomena.

The quantification of terrain volume changes is based on the distance between at least two DTMs, which capture the terrain features at different moments in time (Abelán et al., 2011; Meng et al., 2021). The raster approach, which calculates height differences between identical grid cells (Woolrad & Colby, 2002; Mitasova et al., 2009; Sailer et al., 2012), is frequently employed in volume change analyses. This method is especially appropriate for planar terrains without notable fragmentation in the vertical dimension (e.g., surface inclinations over 60 degrees) or dramatic elevation changes, such as rock walls.

Conversely, for terrains with vertical dissections like rock walls, overhangs, and caves, 3D polyhedral networks or mesh models are utilized in DTM creation. These models better express the nuanced complexity of terrain shapes (Peytavie et al., 2009; Mancini et al., 2017; Gallay et al., 2018). There is an abundance of software and toolboxes available for volume change analysis. From a theoretical-methodological perspective, these tools utilize methods that determine the Euclidean distance in set directions (for instance, along the Z-axis or the shortest distance within a specified search window) between two raster layers (DoD) (Williams, 2012), point clouds (C2C) (Girardeau-Montaut et al., 2005), a combination of a point cloud and mesh (C2M) (Barnhart & Crosby, 2013), or different directions using a multiscale model. This multiscale model compares two point clouds to identify corresponding properties of normal vectors (M3C2) (Lague et al., 2013).

Furthermore, varying LoSR of DTM are employed for volume change estimations, heavily influenced by the quality of the input data used to produce the DTM and the scope of the territory being examined. Consequently, disparate LoSRs of DTM, data structures, and volume change estimation methodologies can yield divergent results.

The paper at hand focuses on calculating the volume changes of a landslide observed over a 5-year monitoring period. Comprehending the dynamics of river sediment input, transport, and deposition is vital for identifying sediment fluxes, assessing sediment budgets, and effectively managing river systems (Rusnák et al., 2020). The monitored landslide is typified as an undercut vertical cliff adorned with overhangs and multiple slopes exceeding 60 degrees in steepness (Figure 2). Such characteristics imply that conventional methods for calculating landslide volume changes using a raster approach might introduce some level of error in the volume computations. Additionally, variations in volume estimations can also be influenced by the properties of the DTM data structure and its LoSR.

Given this background, our primary research queries were:

- How does the chosen method for volume change computation influence the resulting estimate? In this study, we juxtapose two methods for calculating landslide volume changes: one rooted in comparing raster layers (R2R) and the other using 3D mesh models (M2M). Both methods portray the landslide terrain at two distinct moments.
- How does the spatial resolution of the input data affect volume estimation? For this, we began with the hypothesis that as the spatial resolution of input data layers increases, the chosen method's impact on volume change discrepancy would be more pronounced. Yet, there exists a spatial resolution threshold for input layers where the selected method's influence on landslide volume change calculations becomes negligible.

2. Study area

The landslide area is located on the left bank of the Belá River, near the towns of Liptovský Hrádok and Vavrišovo village, in the northern part of Slovakia, specifically in the Liptov region (Figure 1).

The Belá River originates from the confluence of the Tichý and Kôprovský potok Brooks near Podbanské Village and contributes to landslide formation in the area. It drains the mountainous regions of both the High Tatras and a significant portion of the Western Tatras Mountains. The river's basin covers an area of 244 km², with elevations ranging from 630 meters above sea level (at the confluence with the Váh River) to 2494 meters above sea level (along the ridge of the High Tatras). The landslide under investigation spans approximately 5,100 m² and is situated about 6 km upstream from where the Belá and Váh rivers meet (see Figure 1a). The landslide's lowest point, at 691 meters above sea level, is located at the edge of the Belá River, while its highest point reaches 725 meters above sea level at the landslide crown, presenting a relative elevation difference of 34 meters.

The examined area comprises clay loams derived from the less resistant calcareous claystones of the Huty formation (inner-Carpathian Paleogene), overlaid by coarser glacialuvial sediments (Nemčok et al., 1994). The lower section of the cliff, in contact with the river channel, is covered with Holocene gravel sediments. This geological structure, along with the geotechnical properties of the rocks and various hydraulic and climatic factors, contributes to slope instability, increasing both erodibility and material movement into the channel. While the tree vegetation on the leveled terrace at the top of the landslide, primarily consisting of pines and spruces with shallow root systems, does offer some erosion resistance, its impact on subsoil compaction is limited (Zhang et al., 2022).

Vegetation, geological settings, and lateral erosion of the Belá River are primary drivers that determine the



Figure 1. The location of the study area – a landslide-cut cliff at the Vavrišovo site in the Liptov region, Slovakia. The landslide was undercut by the lateral activity of the Belá River (B). Part C illustrates the locations of the scanning positions (marked with red triangles), the computational extent for creating the Digital Terrain Model (DTM) (indicated by a grey dashed line), and the computational extent for volume change analysis (outlined in red)

evolution of landslides and cliff retreat. The central part of the landslide is formed by a slope that does not exceed 45° , with a gradual change in inclination. Conversely, steep slopes with an inclination of more than 60° cover approximately 20% of the landslide area (Figure 2). These parts are located at the foot of the landslide slope near the riverbed and are created by the river's erosion of landslide accumulation. Similarly, steep slopes are also connected with the upper part of the landslide in the detachment zone of the main scarp. The upper part of the landslide and its crown edge are partially covered by tree vegetation. The root system of these trees ensures the compaction of sediments and soil to a certain depth, but on the other hand, it destabilizes the main scarp with overhanging blocks.

3. Methods and data

3.1. Methodological approach

The analysis of volumetric changes in the studied landslide was conducted using terrestrial laser scanning (TLS) data obtained from two mapping campaigns in June 2016 and June 2020. The data layers for volumetric change analysis included TLS point clouds, which were used to derive DTMs in the form of 2D raster models and 3D polyhedral models (3D mesh models). To evaluate the impact of different Levels of Spatial Resolution (LoSR), DTMs with spatial resolutions of 0.1 m, 0.25 m,

0.5 m, 1 m, and 2 m were used. These DTMs were derived from the filtered point cloud. For creating the DTM at a spatial resolution of 0.1 m, classified points from individual mapping campaigns representing the terrain were used based on the original, unfiltered point clouds. For DTMs with spatial resolutions of 0.25 m, 0.5 m, 1 m, and 2 m, input points with respective spatial resolutions of 0.05 m, 0.1 m, 0.2 m, and 0.5 m were utilized. The spatial extent of all point clouds for calculating volume changes was defined by a uniform polygon, which extended 5 m beyond the investigated landslide area. This was done to eliminate the edge effect when generating DTMs. The generated DTMs were then clipped to the polygon of the landslide area under investigation. Subsequently, volumes for DTMs representing each LoSR were estimated, and volume changes during the monitored period were analyzed. The methodological procedure is illustrated in Figure 3.

3.2. Data collection and TLS raw data processing

Mapping campaigns were carried out in June 2016 and June 2020. Data collection was performed using a RIEGL VZ-1000 terrestrial laser scanner. During both mapping campaigns, 10 scan positions were established, with 7 positions located on the upper edge of the landslide and 3 scan positions on the right bank of the Belá River, opposite the landslide.

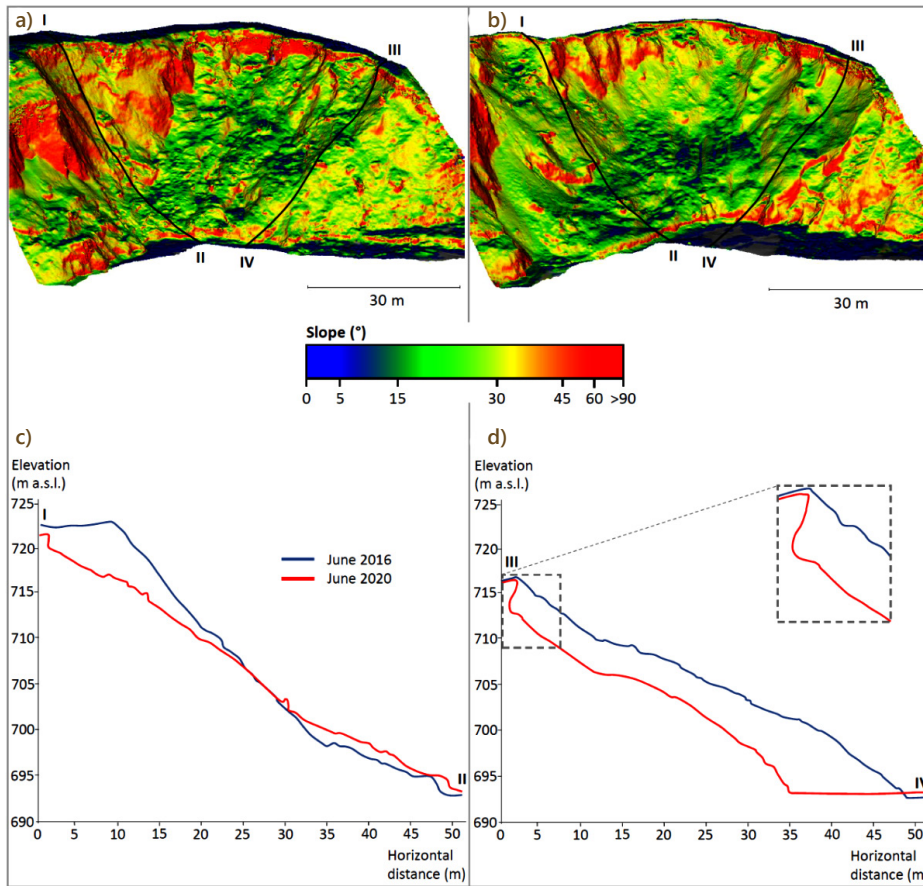


Figure 2. The slope of the area of interest in 2016 (a) and 2020 (b). Vertical profiles through the selected terrain parts (c, d) show terrain topography change during the monitored period

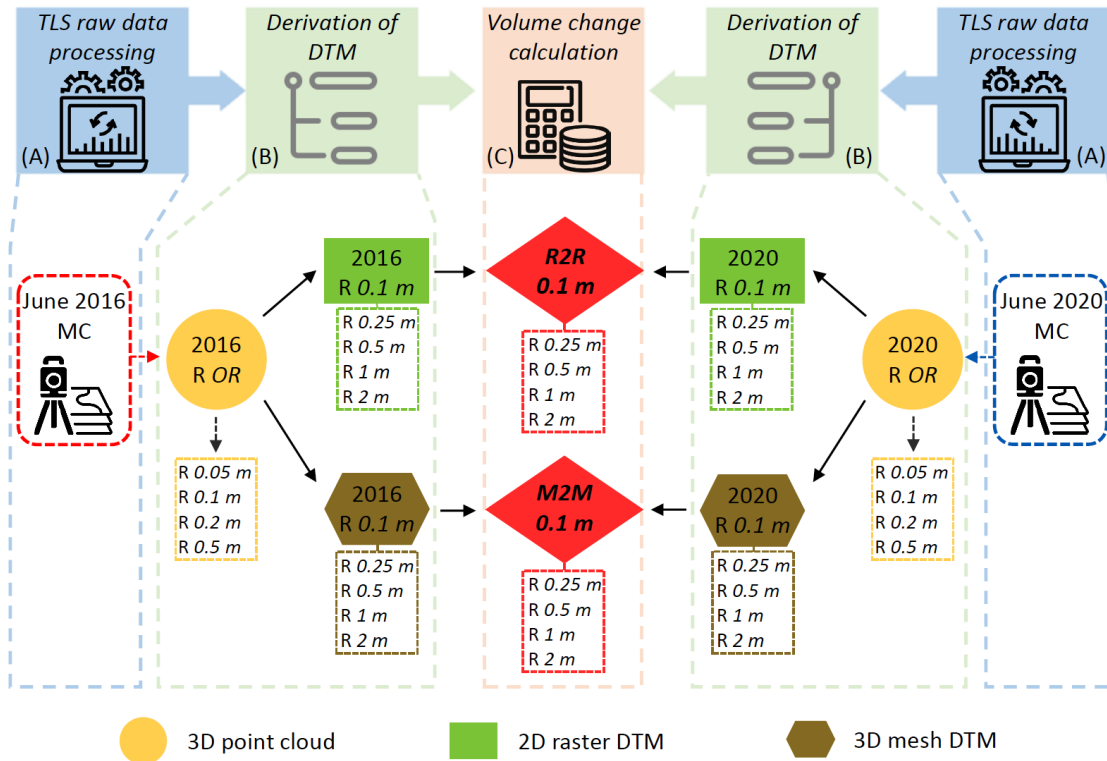


Figure 3. The methodological approach of the point cloud processing from two mapping campaigns (MC) and DTM creation, as well. Dashed line rectangles show the spatial resolution of input point clouds derived from the original point cloud resolution (R OR) and the spatial resolution of created 2D and 3D DTMs

The placement of scanning positions was strategically chosen to eliminate obscurations of terrain forms and vegetation on the landslide, which appear in the resulting point cloud as dropouts of points or unmapped parts of the surface (Figure 1c). Due to the relatively small range of the area of interest, the scanner's range was limited to 450 m, and the laser pulse emission frequency was set to 300 kHz, achieving an effective measurement rate of 122,000 pulses per second. The 'Panorama 60' parameter was also defined, whereby the scanner emits a laser pulse every 0.06° in both vertical and horizontal directions. This spacing results in a point distance of 6 cm at 100 m from the scanner and determines the density of the resulting point cloud.

Part of the data collection involved measuring the position of reference points using the Topcon HiPer II GNSS device. The position of these reference points was determined using differential position measurement in RTK mode, connected to the Slovak real-time positioning service (SKPOS). In total, 4 signaling targets were placed around the scanning positions, and their 3D positions were targeted by the GNSS device. The coordinates of these targets were used to transform the resulting point clouds from both mapping campaigns into a common coordinate system, specifically the S-JTSK projection coordinate system (EPSG code: 5514) and the Baltic vertical datum after alignment (EPSG code: 8357). The TLS data were processed in RISCAN PRO software. This processing involved mutual registration – joining point clouds from individual scanning positions into a single point cloud. The standard deviation of registration of point clouds from individual campaigns was 0.004 m (June 2016) and 0.020 m (June 2020), while the standard deviation of registration into the unified S-JTSK coordinate system and vertical datum was 0.029 m (June 2016) and 0.025 m (June 2020), respectively.

The classification of points was processed in two steps due to the character of the research area and the variety of terrain features, which included significant vertical fragmentation, the occurrence of overhangs, and varying vegetation, including lying tree trunks. First, an automatic object classification algorithm was used, filtering out points with a high degree of position uncertainty and noise. In this step, a Deviation filter with a threshold value of ≤ 40 was applied, removing points with a high deviation from the ideal laser pulse trace (Šupinský et al., 2019). Secondly, points that did not represent the terrain were manually removed, as automatic filtering methods were not entirely effective in areas with lying tree trunks and overhangs. Almost 70% of points from individual mapping campaigns were removed through filtering. The remaining points formed the input data layers for the creation of DTMs and subsequent volumetric analyses.

3.3. Derivation of DTMs with different spatial resolution

In the next phase of our research (Figure 3b), we focused on deriving DTMs from point clouds. To address our re-

search questions, we created two basic types of DTMs from these point clouds: a) 2D raster models and b) 3D mesh models, each at different Levels of Spatial Resolution (LoSR). Specifically, we utilized DTMs with spatial resolutions of 0.1 m, 0.25 m, 0.5 m, 1 m, and 2 m. When preparing point clouds for each LoSR of DTM, we adhered to the principle that the input elevation point field should possess a spatial resolution four times greater than that of the resultant DTM (Hengl, 2006) (as shown in Figures 4a and 4b). Concurrently, we examined how the lower density of the input point cloud, and consequently the lower spatial resolution of the DTM, would affect the accuracy of the estimated volume of the observed landslide. This aspect is crucial for understanding the data quality requirements necessary for effective long-term monitoring of landslides.

For the spatial resolution of the DTM at 0.1 m (Figure 4c), we employed the original density of the point cloud (Figure 4a). DTMs with spatial resolutions of 0.25 m, 0.5 m, 1 m (Figure 4d), and 2 m were derived from point clouds thinned to respective levels of 0.05 m, 0.1 m, 0.2 m (Figure 4b), and 0.5 m. This reduction in point clouds was achieved through controlled filtering using the Space method and the Cloud subsampling tool in CloudCompare software (CloudCompare, 2022).

The computational region for deriving the DTMs was set to match the extent of the input point clouds. However, for determining volume changes, a smaller scope was defined. The shape and extent of this polygon were based on the spatial extent of the landslide in 2020, reflecting the significant loss of landslide mass and transformation of its boundaries between 2016 and 2020. The computational area for volumetric analysis was selected by trimming the resulting DTMs according to the polygon depicted in Figure 1c (indicated by the red line).

The raster DTMs were derived using the *blast2dem* tool in the *LAStools* software (LAStools, 2023). For 3D mesh models, we first calculated the normals of the input point clouds using the *Compute normals* tool in *CloudCompare* software. The orientation of these normals was determined using the *triangulation local surface model* and the *k-Nearest Neighbors* algorithm with a value of 10 (Mucherino et al., 2009). All datasets underwent visual inspection to ensure that normals were correctly oriented from the surface. The 3D mesh models were then derived using the *Poisson Surface Reconstruction* tool in *CloudCompare* software (Kazhdan et al., 2006), with the spatial resolution set as required (0.1 m for Figure 4e, and 0.25 m, 0.5 m, 1 m for Figure 4f, and 2 m) through the "Resolution" parameter setting.

We calculated the standard statistical parameters, such as average, median, minimum, and maximum values, for individual models across different data structures and resolutions. To analyze similarities or differences between the models (raster and 3D mesh), we used the most detailed model, i.e., the model with a spatial resolution of 0.1 m, as a reference. This statistical analysis assessed differences in elevations at identical locations across the models.

For raster data structures, we calculated the differences between individual grid cells of the reference DTM (0.1 m) and the DTM representing the given LoSR using the Raster calculator tool in ArcGIS Pro. In the case of the 3D mesh data structure, we derived point clouds from the individual models. Then, we calculated the elevation differences between points of the reference 3D mesh model and the model representing the specified spatial resolution using the Compute cloud to mesh distance tool in CloudCompare software.

In both cases, outliers were subsequently removed. This meant that the resulting statistical indicators were cleaned by excluding the percentiles of extreme values in both the positive and negative segments.

3.4. Determining the area of surfaces, volumes, and volume changes

For the evaluation of the volumetric analysis, we compared the raster and mesh DTM approaches, focusing on how the specific characteristics of each data structure influence the estimation of volumes and the detection of surface areas.

The fundamental characteristic of raster-based DTMs is that they are regular, positionally localized matrices of

elevation values. They have a defined raster extent, cell size, number of rows and columns, and a reference coordinate system. Raster-based DTMs are essentially two-dimensional but can be visualized in 3D space. The area of raster DTMs is calculated based on the product of the number of cells and the cell size. However, there are methods for determining the 3D area of terrain derived from raster data, such as the Surface Volume tool in ArcGIS Pro 3.1.0 (ArcGIS Pro, 2023) or `r.surf.area` in GRASS GIS 7.8.7 (GRASS GIS, 2022). These methods involve deriving a point cloud from grid cells (cell centroids), creating a TIN model, and then calculating the area of the 3D DTM surface. The calculation of volumes from raster data is the sum of the areas of the raster cells and their heights, with tools like Surface Volume in ArcGIS Pro, `r.volume` in GRASS GIS, and Compute 2.5D volume in CloudCompare 2.12.4 being designed for this purpose. However, when calculating volume from rasters, the course of the TIN surface is not considered.

For mesh DTMs, we used a TIN DTM represented by a spatially distributed set of triangles that approximate the terrain's shape. The technical documentation specifies that the construction of the triangle network is limited to ensure that no more than one triangle occupies the same location, and no triangle has a vertical side (perpendicular

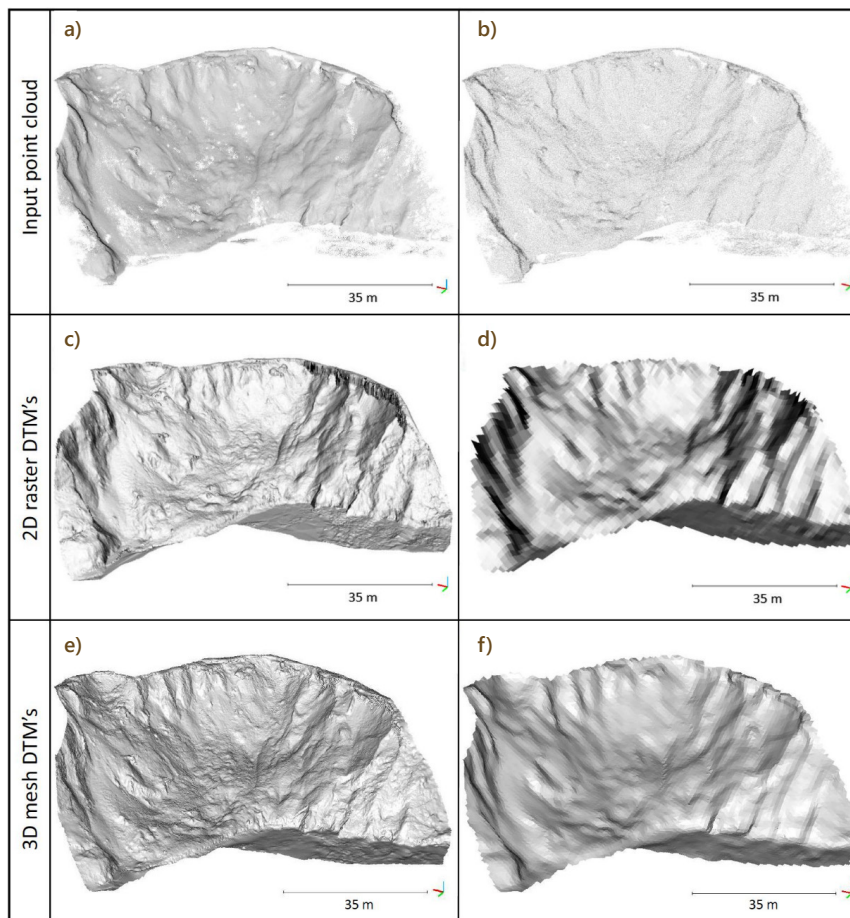


Figure 4. Comparison of the level of detail of the input point clouds in full resolution (a) and after subsampling of point clouds with a step of 0.2 m (b), derived raster models with a spatial resolution of 0.1 m (c) and 1 m (d) and derived 3D mesh models with a spatial resolution of 0.1 m (e) and 1 m (f)

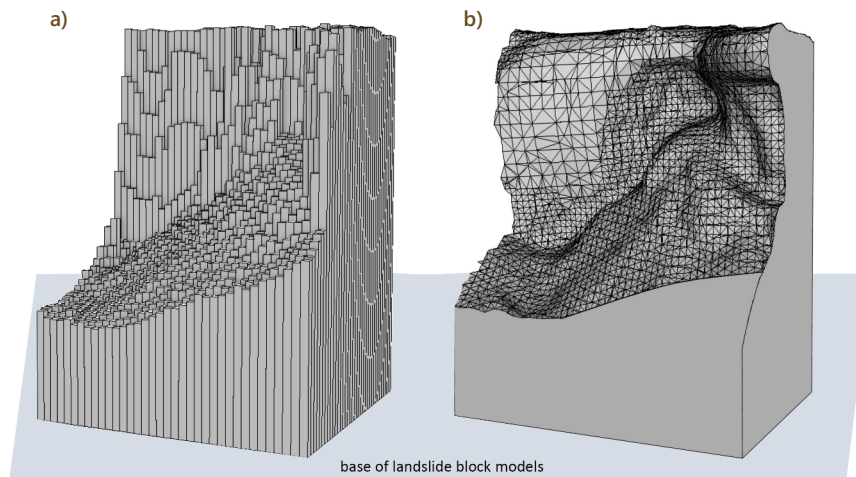


Figure 5. Schematic visualization of raster (a) and 3D mesh (b) landslide block models. For the creation of landslide block models at different LoSR, the base with the same elevation was used

to the plane defined by the X and Y axes). This means that for any given X and Y values, there can only be one elevation value in the TIN model. However, this limitation does not apply to the 3D mesh data structure, as the expression of the terrain surface is not constrained by the number of elevation values for unique X and Y values. Therefore, the calculation of the surface area of mesh models is based on the sum of the areas of the individual triangles. Moreover, for 3D mesh models, the volume is determined as the sum of the volumes of tetrahedrons (three-dimensional objects with a triangular base defined by another vertex on the opposite side of the object). From this perspective, modeling the terrain using a raster structure can be considered a 2D approach, while using a mesh data structure represents a 3D approach (Figure 5). In this context, we also focused on detecting the surface area from both 2D raster and 3D mesh models, as well as estimating the volumes derived from both data structures.

The volume calculation based on the Mesh-to-Mesh (M2M) approach was conducted using 3D mesh models. The first step in deriving 3D mesh models of the landslide block involved generating bases for these models. This process, which was carried out in Blender software (Blender, 2018), created models that represented the mass of the landslide block from the 3D mesh DTM. In Blender, the imported 3D mesh terrain models were negatively extruded by 50 meters in the Z direction. To ensure consistency between individual 3D mesh models representing different time points, we created an auxiliary 3D mesh cube. The top wall of this cube served as a reference plane, set at an elevation of 690 meters above sea level.

These modified 3D mesh models, along with the created cube model, were then imported into MeshLab software (Cignoni et al., 2008). Using the geoprocessing tools of the libigl library (Zhou et al., 2016), which is integrated into MeshLab, we calculated the difference between the 3D mesh model of the area of interest and the auxiliary cube. This procedure resulted in a database of 3D mesh models, each having a surface with a base at the reference

level, representing the landslide at various defined spatial resolutions. The volume of these models was calculated using the Compute Geometric Measures tool (Mirtich, 1996) in MeshLab.

Finally, the resultant change in volume was determined by subtracting the volumes at individual time points. The results were then evaluated based on the type of data structure used and the LoSR. To accurately compare volumes or changes in volume, it is crucial to ensure that the extent of the study area remains consistent. In the case of a 2D raster model, determining the extent is straightforward due to the geometric structure of this data format. However, with 3D mesh models, changes in the area can occur both over time (comparing data from 2016 and 2020) and across different spatial resolutions (0.1, 0.25, 0.5, 1, and 2 meters). To prevent inconsistencies between the 3D mesh model and the 2D raster model, we ensured that the extent of the study area was identical across all input datasets.

4. Results and discussion

To rigorously answer the research questions concerning the estimation of volumetric changes in the landslide, it is essential to analyze the impacts of the data structure and spatial resolution of the DTM, as well as the effects of specific terrain features.

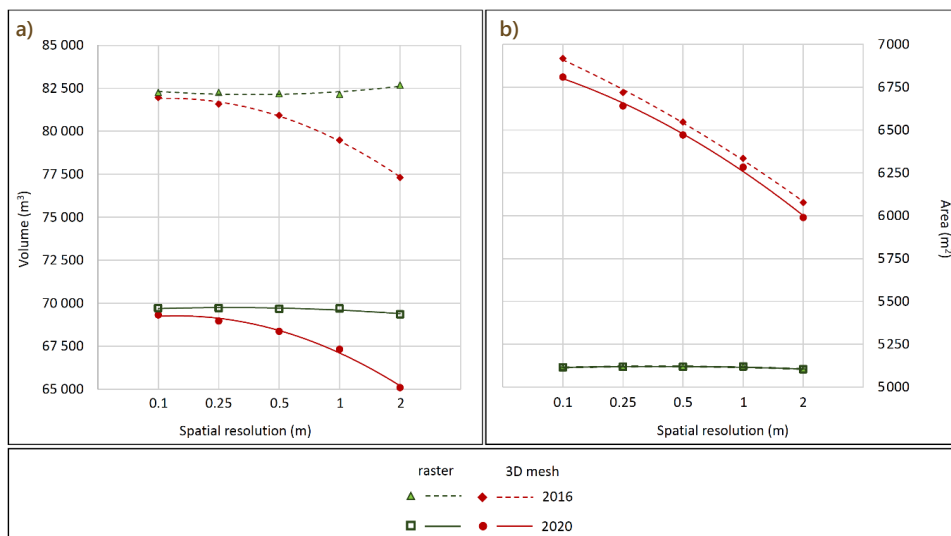
4.1. Analysis of the data structure impact and spatial resolution of the DTM on the estimation of the volume change of the landslide

4.1.1. Evaluation of DTM and spatial resolution for calculating the surface area and volume of the landslide mass block

Table 1 and Figures 6a and 6b present the results of the calculated area of the landslide surface and the volume of the landslide mass block in 2016 and 2020.

Table 1. Estimated values of landslide material volume and landslide terrain surface area expressed using 3D mesh and raster model at different LoSRs

Spatial resolution (m)	2016				2020			
	3D mesh		Raster		3D mesh		Raster	
	Area (m ²)	Volume (m ³)	Area (m ²)	Volume (m ³)	Area (m ²)	Volume (m ³)	Area (m ²)	Volume (m ³)
0.1	6917.89	81 964.09	5115.73	82 267.22	6810.10	69 322.03	5115.73	69 709.73
0.25	6719.27	81 586.81	5118.31	82 262.96	6641.24	68 967.91	5118.31	69 712.59
0.5	6547.42	80 932.64	5118.75	82 192.83	6471.46	68 363.30	5118.75	69 668.60
1	6334.96	79 486.81	5120.00	82 147.43	6283.41	67 324.64	5120.00	69 696.51
2	6077.03	77 312.97	5104.00	82 689.32	5989.82	65 093.71	5104.00	69 353.30

**Figure 6.** Estimated landslide mass block volume (a) and landslide terrain surface area (b) expressed using 3D mesh and raster model at different LoSRs

Our results indicate that when calculating the area of the landslide surface, a slight change occurs with varying spatial resolution. This change in area is associated with the shape of the territory, the different sizes of the grid cells, and the total number of cells in a given spatial resolution. Although the 2D surface area corresponds to the area of the polygon (Figure 1c, red line), the area is altered due to the effect on the edges of the raster in grids, partly due to the change in spatial resolution and the varying number of differently sized cells within the extent, influenced by rotated and irregular shapes.

In contrast, the 3D mesh models exhibit more significant changes in the area of the landslide surface at different resolutions. As the spatial resolution decreases, the surface area of the landslide also gradually diminishes. This is because higher spatial resolutions allow for more detailed recording of smaller terrain forms, increasing the surface area of the 3D mesh DTM. Conversely, with lower spatial resolution and reduced level of detail, the surface area decreases. The 3D mesh approach also captures overhangs, landslide blocks, and gravels with detailed geometric structures in high spatial resolutions (up to 0.5 m). The change in the total area of the landslide between 2016 and 2020 also reflects transformations in the landforms.

The landslide volume calculations revealed three main findings:

- 1) The raster data structure does not show a dependence between the spatial resolution of the models and the estimated volume (Table 1, Figure 6). Therefore, changing the spatial resolution of the raster does not significantly affect (less than 1%) the calculation of the landslide mass block volume.
- 2) The 3D mesh data structure, however, reflected changes in spatial resolution in volume estimation. This can be attributed to changes in the landslide area, directly impacting the volume calculation. Thus, a smaller surface area is associated with a lower volume estimate.
- 3) The overall estimated volumes are overestimated by the raster data structure compared to the 3D mesh data structure. Higher overestimation up to the 0.5 m level is linked to better representation of overhangs, which are not captured by the raster data structure. In raster models, overhangs are often modeled as vertical walls due to the use of bivariate functions in surface generation (Mitášová & Mitáš, 1993; Florinsky & Pankratov, 2016). Increasing generalization from 1 m spatial resolution

has a smaller effect on volume calculation because of the application of the Poisson interpolation function (Kazhdan et al., 2006), which more accurately captures surface trends and landform shapes. Ultimately, 3D mesh surfaces provide a more precise estimate of landslide volume compared to raster models.

The selected statistical indicators (Table 2) revealed that raster DTMs with a grid size up to 1 m demonstrate a high degree of similarity. This similarity is evident in the median values and the proportional distribution of values in both positive and negative segments. More significant differences become apparent only in DTMs with a spatial resolution of 2 m. Generally, as spatial resolution decreases, the range of values tends to gradually increase. The deviation in values can be gauged by comparing the elevation differences between the minimum and maximum values across individual resolutions. For raster data structures with resolutions up to 1 m, the distribution of elevation differences is minor (up to 2%). Elevation changes within these models are within ± 0.5 m and are evenly distributed across both positive and negative sectors, influencing the overall volume change between different levels and indicating higher detection quality. Although local differences in elevations exist between individual LoSR in raster models, these are typically offset by neighboring cells, which exhibit opposite elevation differences.

For the 3D mesh data structure with resolutions up to 1 m, the minimum and maximum values reached ± 0.2 m, suggesting a high similarity between these models. However, the range of values between positive and negative segments is larger (around 5%) compared to the raster

data structure, as reflected in the average and median values. Although the values are very similar and close to zero for resolutions up to 1 m, there is a noticeable increasing trend attributable to the nature of the interpolation function used during DTM creation. This greater disparity in the distribution of values between the positive and negative segments leads to a cumulative effect in elevation values, predominantly in the positive segment for our case. Consequently, this affects the larger difference in the estimation of the landslide mass volume. Therefore, in our study, the estimated volume value decreases as the LoSR of the 3D mesh model decreases.

4.1.2. Evaluation of volume changes for the monitored period

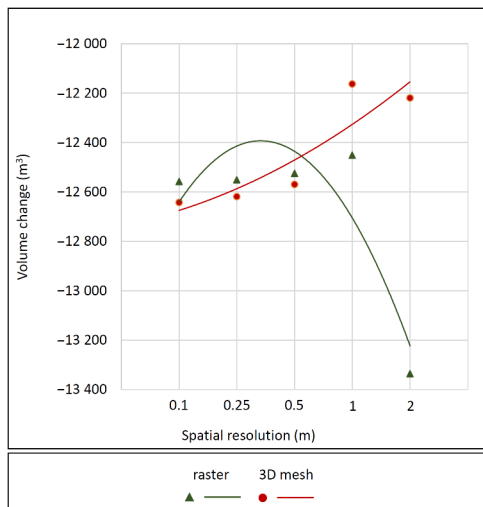
During the selected period, raster data structures with grid sizes up to 1 m indicated an erosion of approximately 12,500 m³, with a negligible difference between LoSR of ± 50 m³ (less than 0.5% of the total estimated volume change). Consequently, it can be inferred that using raster models up to a resolution of 1 m allows for volume estimates that are less dependent on the DTM's spatial resolution. For grid sizes of 2 m, however, significant errors were observed. Echoing the findings of Štroner et al. (2019), we note that changing the spatial resolution of the cell size to 1 m did not significantly impact the result of the volume change estimation (Table 3, Figure 7). The most notable differences in volume were observed at the 2 m resolution, where surface smoothing due to interpolation methods was evident. Additionally, the significant discrepancy in volume change at a spatial resolution of 2 m resulted in larger differences in volumes between 2016 and 2020

Table 2. Selected statistical parameters of the analysis of height differences between the reference DTM and DTM's in the selected LoSRs

	DTM resolution	Count (98%)	Average	Median	Min	Max	Count in the positive segment	Count in the positive segment (%)	Count in the negative segment	Count in the negative segment (%)
R2R 2016	0.25–0.1 m	499 894	–0.003	–0.001	–0.276	0.228	244 416	48.89	255 478	51.11
	0.5–0.1 m	499 894	–0.002	0	–0.448	0.417	246 451	49.30	253 443	50.70
	1–0.1 m	499 894	–0.004	–0.002	–0.809	0.777	245 110	49.03	254 784	50.97
	2–0.1 m	499 894	0.014	0.010	–2.189	1.893	256 303	51.27	243 591	48.73
R2R 2020	0.25–0.1 m	501 341	–0.003	0	–0.261	0.201	246 264	49.12	255 077	50.88
	0.5–0.1 m	501 341	–0.002	0	–0.424	0.379	248 473	49.56	252 868	50.44
	1–0.1 m	501 341	–0.003	–0.001	–0.778	0.737	248 579	49.58	252 762	50.42
	2–0.1 m	501 341	0.029	0.023	–1.897	1.701	270 354	53.93	230 987	46.07
M2M 2016	0.25–0.1 m	305 098	–0.002	–0.001	–0.078	0.056	144 040	47.21	161 058	52.79
	0.5–0.1 m	287 728	–0.003	–0.002	–0.135	0.099	135 381	47.05	152 347	52.95
	1–0.1 m	273 905	–0.004	–0.002	–0.236	0.186	132 557	48.40	141 348	51.60
	2–0.1 m	260 833	0.046	0.052	–0.486	0.53	150 877	57.84	109 956	42.16
M2M 2020	0.25–0.1 m	300 912	–0.003	–0.001	–0.109	0.057	139 808	46.46	161 104	53.54
	0.5–0.1 m	284 245	–0.006	–0.003	–0.155	0.097	129 043	45.40	155 202	54.60
	1–0.1 m	271 533	–0.006	–0.004	–0.22	0.184	127 041	46.79	144 492	53.21
	2–0.1 m	257 217	–0.004	–0.005	–0.371	0.363	124 341	48.34	132 876	51.66

Table 3. Volume changes in the monitored period at defined LoSRs and selected data structures (raster and 3D mesh)

Spatial resolution (m)	R2R			M2M		
	Total volume change (m ³)	Volume change compared to 0.1 m spatial resolution (m ³)	Volume change compared to 0.1 m spatial resolution (%)	Total volume change (m ³)	Volume change compared to 0.1 m spatial resolution (m ³)	Volume change compared to 0.1 m spatial resolution (%)
0.1	-12 557.49	0	0	-12 642.06	0	0
0.25	-12 550.37	7.12	-0.06	-12618.90	23.16	-0.18
0.5	-12 524.23	33.26	-0.26	-12 569.34	72.72	-0.58
1	-12 450.92	106.57	-0.85	-12 162.17	479.89	-3.80
2	-13 336.02	-778.53	6.20	-12 219.26	422.80	-3.34

**Figure 7.** The volume changes of landslide for raster and 3D mesh model

(Table 1, Figure 6), leading to greater uncertainty in the DTM relative to the actual terrain.

In contrast, the 3D mesh data structure recorded erosion of approximately 12,642 m³ at a resolution of 0.1 m. The smallest volume change was estimated at a resolution of 1 m (12,162 m³). The difference in volume changes between individual LoSRs gradually increased, from 0.18% at a spatial resolution of 0.25 m to 3.8% at 1 m, with the largest error increase observed when moving from 0.5 m to 1 m resolution (from 0.58% to 3.80%). These differences in volume changes across spatial resolutions depend on the DTM's ability to capture specific terrain features at a given moment.

When comparing volume changes between raster and 3D mesh data structures across different spatial resolutions, it was found that higher resolutions (up to 0.5 m) in 3D mesh models can record the volume of change more precisely (approximately 85 to 45 m³ difference). The 3D mesh model accurately captures the detailed geometric structure of terrain features, including specific elements like overhangs. At a spatial resolution of 0.5 m, both models are comparable, with a minimal value difference of about 45 m³ (0.35%). For this type of landform structure, at a resolution of 0.5 m, the area has minimal impact on the choice of model for calculating volume change. However, at resolutions up to 1 m, the raster structure's

results are similar to those of higher spatial resolutions (up to 0.85% difference). The decrease in resolution led to an increasing discrepancy in volume change, which can be attributed to greater generalization of terrain features in raster models, the edge effect (Wade et al., 2003), and increased uncertainty in rendering the landslide surface, subsequently affecting volume determination.

4.2. The influence of specific terrain features on the estimation of volume change at different levels of spatial resolution

4.2.1. Slope of the landslide body (SLB)

The main body of the landslide and its slope (SLB) together account for over 95% of the landslide's total area. The SLB is characterized based on morphometric analyses, which identify it as an area with continuous elevation changes and without any abrupt changes in gradient (defined as a change exceeding 90°). The gradient here refers to the vector of the first derivatives of the scalar function in the direction of the slope. This part of the landslide is composed of the lower accumulation zone and the central transportation zone.

For a detailed comparison, we focused on a selected sector in the central part of the landslide, measuring 10×10 meters, as shown in Figure 8. In this specific region, only the erosion of material was observed, indicated by negative differences in elevation. Notably, our statistical analyses were not influenced by any compensation between positive and negative values.

The results for the Slope of the Landslide Body (SLB) were found to be similar to those of the entire landslide (Table 1, Figure 6b). In the raster data structure, the model area remains constant due to the grid cell size being fixed and aligned with the axes of the coordinate system, without any rotation. Conversely, the 3D mesh data structure shows temporal variation, mainly attributed to surface erosion and changes in microforms. This variation is observable up to a spatial resolution of 0.5 m in the 3D mesh DTM. As the spatial resolution is reduced, the smallest terrain forms begin to disappear.

The area extent of the 3D mesh demonstrates temporal changes due to surface erosion, an effect that is closely related to the model's resolution. This implies that the change in area extent is significant enough to surpass the detection limits imposed by the resolution of the model.

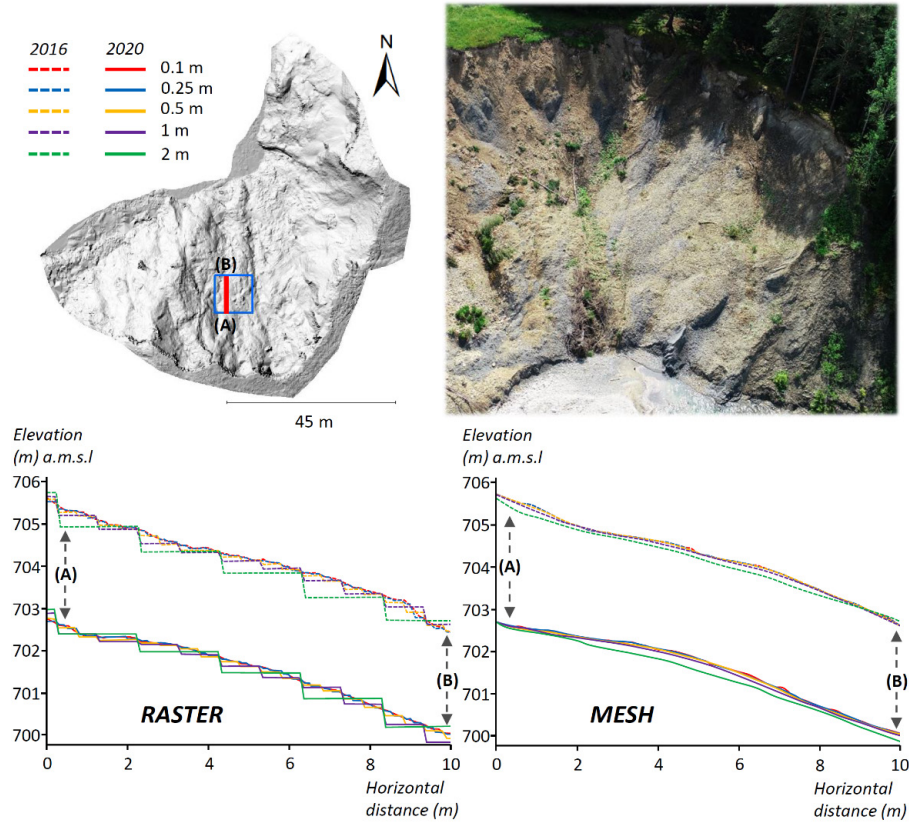


Figure 8. The blue box shows the selection of the landslide part for the analysis of the terrain form of the slope. The red line shows the position of the profiles. The photo captures the state of the landslide in 2016. In the lower part of the image, there are profiles for individual LoSRs and data types. The dashed line is the recorded terrain profile for 2016 and the solid line for 2020

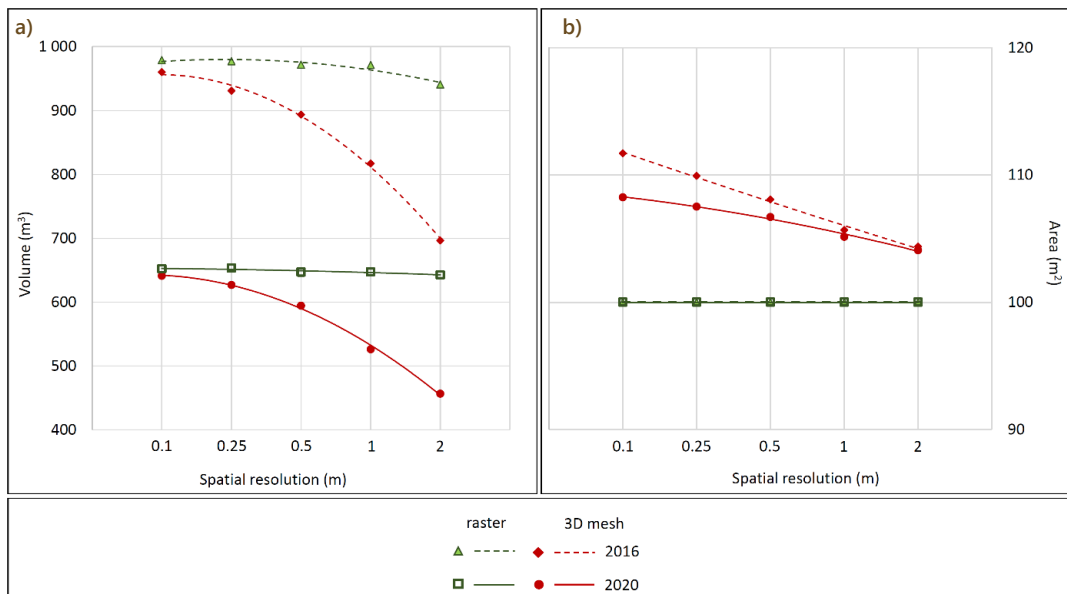


Figure 9. Estimated volume of the landslide mass block (a) and the area of the landslide terrain surface (b) expressed using a 3D mesh and a raster model at different LoSRs – the slope of the landslide body

Table 4. Values of the area and volume of the landslide mass block for the given spatial resolution and data structure – the slope of the landslide body

Spatial resolution (m)	2016				2020			
	3D mesh		Raster		3D mesh		Raster	
	Area (m ²)	Volume (m ³)	Area (m ²)	Volume (m ³)	Area (m ²)	Volume (m ³)	Area (m ²)	Volume (m ³)
0.1	111.69	960.16	100	979.03	108.25	641.31	100	652.17
0.25	109.93	931.10	100	977.30	107.51	626.83	100	653.49
0.5	108.07	893.59	100	971.99	106.70	594.50	100	647.08
1	105.67	817.02	100	971.41	105.14	526.38	100	647.16
2	104.36	696.60	100	940.88	104.09	456.76	100	642.84

Table 5. Volume change on the slope

Spatial resolution (m)	R2R			M2M		
	Total volume change (m ³)	Volume change compared to 0.1 m spatial resolution (m ³)	Volume change compared to 0.1 m spatial resolution (%)	Total volume change (m ³)	Volume change compared to 0.1 m spatial resolution (m ³)	Volume change compared to 0.1 m spatial resolution (%)
0.1	-326.86	0	0	-318.85	0	0
0.25	-323.81	3.05	0.93	-304.27	14.58	4.57
0.5	-324.91	1.95	0.60	-299.09	19.76	6.20
1	-324.25	2.61	0.80	-290.64	28.21	8.85
2	-298.04	28.82	8.82	-239.84	79.01	24.78

Volume changes in the SLB were calculated at a height of 695 meters above sea level, as shown in Table 4 and Figure 9a. The volume calculations vary between different models at varying LoSRs. For raster DTMs with resolutions up to 1 meter, the impact on volume estimation is not significant. In 2016, the volume ranged from 979.03 m³ to 971.41 m³, with a difference of only 7.62 m³ (less than 1% of the total estimated volume for the selected part of the SLB). In 2020, the estimated volumes varied from

653.49 m³ to 647.08 m³, indicating a difference of 6.41 m³, which is again less than 1%.

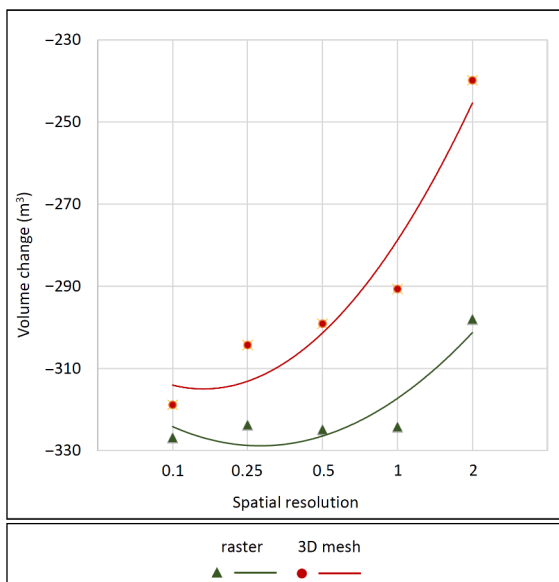
However, at the lowest spatial resolution of 2 meters, there was a significant change in the estimated volume for the year 2016 (by more than 70 m³, equating to over 7.5%). In this instance, the effect of the interpolation function on smoothing out terrain features becomes more pronounced. As a result, the values of terrain heights are underestimated (as depicted in Figure 8 RASTER), leading to a larger discrepancy in the estimated volume when compared to models with a higher LoSR, as detailed in Table 4 and Figure 9.

4.2.2. Overhang

The overhang is a distinctive landform characterized by a significant vertical change in gradient, typically with a slope greater than 90° relative to the horizontal plane. In our research area, this type of landform was predominantly located in the head scarp area. In this region, the presence of trees, with their root systems reinforcing the material to a certain depth, was notable. Below this depth, continuous erosion occurred (Figure 11). Following the collapse of trees along with the undercutting block, the tree trunks, along with the eroded material, gradually slid down towards the river.

Similar to the analysis conducted for the SLB, a specific part of the terrain, measuring 10×10 meters, was selected for detailed analysis of this landform feature (Figure 11).

The area change results for the raster data structure, as shown in Table 6 and Figure 12b, mirror those observed in

**Figure 10.** The volume change on the slope terrain form for the raster and 3D mesh model

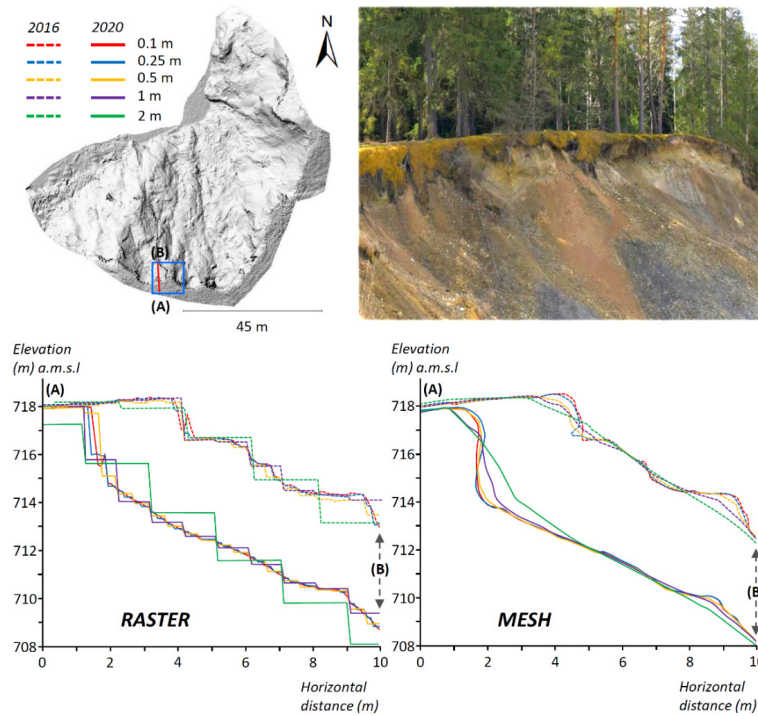


Figure 11. The blue box shows the selection of the landslide part for the analysis of the terrain form of the overhang. The red line shows the position of the profiles. The photo captures the state of the landslide in 2020. In the lower part of the image, there are profiles for individual LoSRs and data types. The dashed line is the recorded terrain profile for 2016 and the solid line for 2020

the analyses of the entire landslide and the SLB. In these cases, the terrain surface area remains constant due to the regular, non-rotated square shape of the extent.

For the 3D mesh DTM surface, we observed a gradual decrease in the surface area up to a resolution of 1 meter, followed by a slight increase at a 2-meter resolution. We attribute this minor increase in surface area to the continuation of the function over the terrain edges, where there is a greater difference in elevation. The interpolation functions, which are based on the input points, behave differently depending on the terrain’s morphometric

characteristics. When the change in elevation is smooth (i.e., without steep changes), the area of the slope surface decreases with lower Levels of Spatial Resolution (LoSR), as this results in the smoothing of terrain microforms. However, when the interpolated surface crosses over a terrain edge, the influence of the interpolation function settings becomes more apparent. In such cases, the modeled surface can exhibit more undulation along these sharp terrain edges, leading to a higher value of the surface area for this part of the landslide. It is important to note that since this analysis focused on a small part of the territory relative

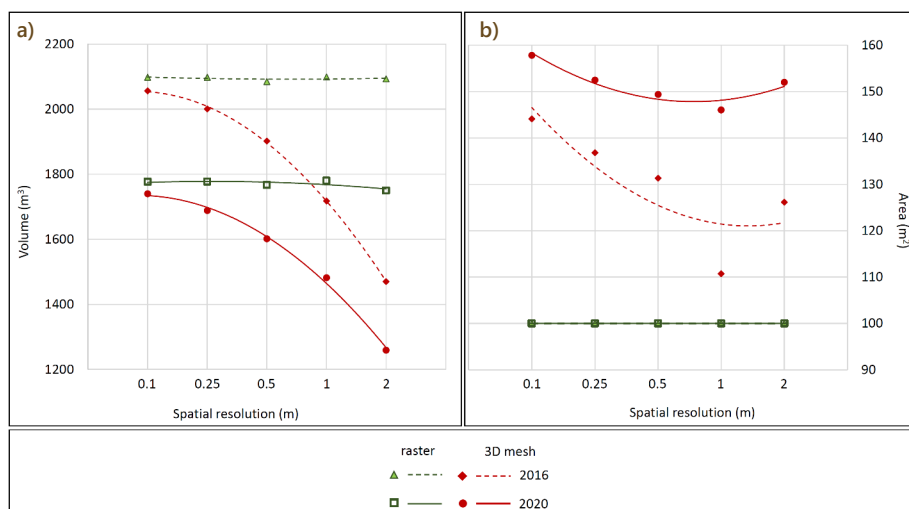


Figure 12. Estimated volume of the landslide mass block (a) and the area of the landslide terrain surface (b) expressed using a 3D mesh and a raster model at different LoSRs – overhang

Table 6. Values of the area and volume of the landslide mass block for the given spatial resolution and data structure – overhang

Spatial resolution (m)	2016				2020			
	3D mesh		Raster		3D mesh		Raster	
	Area (m ²)	Volume (m ³)	Area (m ²)	Volume (m ³)	Area (m ²)	Volume (m ³)	Area (m ²)	Volume (m ³)
0.1	144.12	2056.34	100	2098.02	157.81	1740.13	100	1776.72
0.25	136.82	2000.88	100	2098.25	152.48	1688.67	100	1777.21
0.5	131.30	1901.91	100	2084.53	149.38	1601.91	100	1767.10
1	110.70	1717.93	100	2099.19	146.04	1482.26	100	1780.29
2	126.14	1470.01	100	2093.04	152.01	1259.21	100	1750.20

Table 7. Volume change on the overhang

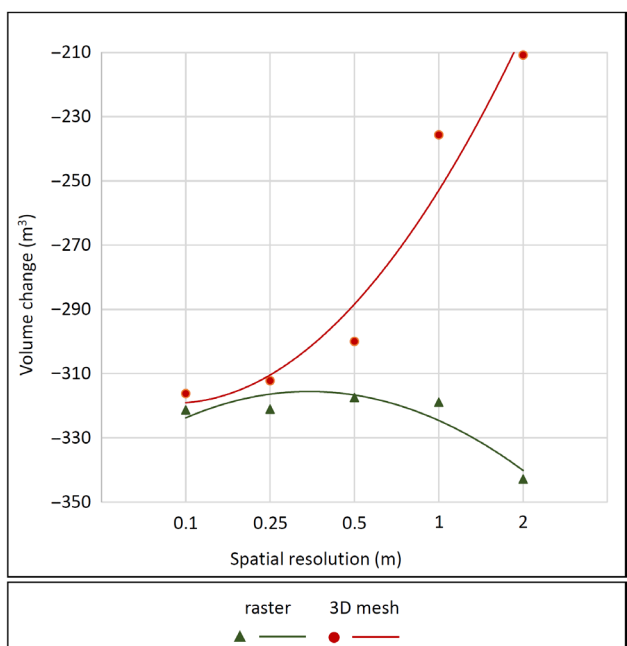
Spatial resolution (m)	R2R			M2M		
	Total volume change (m ³)	Volume change compared to 0.1 m spatial resolution (m ³)	Volume change compared to 0.1 m spatial resolution (%)	Total volume change (m ³)	Volume change compared to 0.1 m spatial resolution (m ³)	Volume change compared to 0.1 m spatial resolution (%)
0.1	-321.30	0	0	-316.21	0	0
0.25	-321.04	0.26	0.08	-312.21	4	1.26
0.5	-317.43	3.87	1.20	-300.00	16.21	5.13
1	-318.90	2.4	0.75	-235.67	80.54	25.47
2	-342.84	-21.54	-6.70	-210.80	105.41	33.34

to the entire landslide, this specific dependence was not observed in the analysis of the entire landslide (Table 1, Figure 6b).

3D mesh data structure reflects more significant changes in the volume for different resolutions (Table 7, Figure 13). Thus, as the LoSR decreases, the value of the estimated volume decreases significantly. In our research area, we noticed a decrease in volume with a gradual decrease in the spatial resolution of the 3D mesh model at the level of approximately 30% for both monitored time periods (from 2056.34 m³ to 1470.01 m³ for 2016, respectively from 1740.13 m³ to 1259.21 m³ for 2020). However, with the decrease in volume for all LoSRs, the question may arise as to why the increase in surface area of this part of the landslide for the 2 m spatial resolution was not also reflected in the increase in volume. We explain (Table 5 and Figure 10) that for the modelled 3D mesh DTM, a diluted point cloud was used as input data, while the interpolation function overran the course of the input point field. On the one hand, there was undulation of the surface, which was reflected in the increase of the surface area, but the resulting surface was located below the values of the input point field, which was reflected in the decrease of the block volume value. In the case of growth models, even in the case of an overhang, there is no significant change in the spatial resolution of the value of the estimated volumes. For the period 2016, we recorded a difference in the estimated value of the volume for individual LoSRs at the level of 14.66 m³, which is approximately 0.7% of the total volume, and for the year

2020, it was a difference of 30.09 m³, which represents approximately 1.7% of the total volume (Table 7).

In both the raster and 3D mesh data structures, erosion of the overhangs is identified as the dominant process affecting volume changes, as detailed in Table 7 and Figure 13. Up to a spatial resolution of 0.25 meters, the differences in volume change between the raster and

**Figure 13.** The volume change on the overhang terrain form for the raster and 3D mesh model

3D mesh models are minimal, with discrepancies up to 4 m^3 . However, as the LoSR decreases, the disparity in volume changes between the two models becomes more pronounced.

Regarding volume change calculations, raster models yield more consistent values. Nonetheless, when compared to the 3D mesh data structure, they exhibit a slight overestimation of volume change, exceeding 1.5%. This overestimation corresponds to a value of more than 5 m^3 . Notably, at spatial resolutions greater than 1 meter, particularly in the 3D mesh data structure, significant changes in the terrain area are observed in comparison to higher LoSRs. At these lower resolutions, the modelled surfaces become excessively smoothed, exhibiting interpolation artefacts. Consequently, these lower-resolution models are deemed unsuitable for accurate estimation of volume changes.

5. Conclusions

Nowadays, technological development and sensor improvement offer new possibilities for mapping and detecting spatial changes. The application of 3D technology has become a fundamental technique for monitoring and assessing landscape change. SfM-photogrammetry also opens new avenues for generating low-cost and precise 3D models. Field surveys with TLS are often combined with SfM-photogrammetry, drone LiDAR survey, or airborne LiDAR to produce a vast amount of data, especially in the form of point clouds. Assessing this type of data, with its high spatial resolution and vertical precision, brings several challenges related to data processing and interpretation. This article aimed to answer two important questions. Firstly, how does the selection of the data model affect the estimation of volume change? Evaluations of (1) raster models (R2R) and (2) 3D mesh models (M2M) were tested and analyzed over two time horizons. Secondly, how does the effect of the spatial resolution of the input data affect the estimation of the landslide mass volume?

An undercut landslide cliff near Vavrišovo in Slovakia was selected for the research and calculation of volume changes. The point clouds obtained from two TLS campaigns in June 2016 and June 2020 were used as the source data for creating DTM in two data structures – 2D raster and 3D mesh. Before creating DTMs for different spatial resolutions, the input point cloud was classified and then spatially optimized. With this step, terrain models representing the landslide at various resolution levels (0.1 m, 0.25 m, 0.5 m, 1 m, and 2 m) were derived from point clouds of differing densities. Based on the presented methodology and the discussed results, we formulate the following observations and findings:

- In the case of a raster data structure, changing the spatial resolution of a raster cell does not affect the calculation of the surface area of the investigated object since it is a 2D surface. The change in surface area is caused by the irregular shape of the extent

and is related to the edge effect in the creation of the cell structure of raster models (irregular extent for whole landslide analyses). In the case of the analysis of specific terrain forms, regular and non-rotated polygons were used, and therefore, in these cases, the marginal effect of the raster models in determining the area of the territory did not manifest itself.

- To determine the area of the landslide surface expressed by a 3D mesh data structure, the LoSR has a significant impact. The surface area is calculated based on the determination of the elementary faces of the mesh structure distributed in 3D space. The higher the LoSR, the larger the surface area is. This is related to the fact that when building a 3D mesh data structure derived from a point cloud, at higher LoSRs (0.5 m to 0.1 m), the geometry of the terrain's microforms is captured in more detail. Thus, a larger number of elementary faces distributed in space is needed to express the course of the terrain. As the spatial resolution decreases, greater smoothing of terrain microforms is applied. In this case, the landslide area decreases for resolutions from 0.1 m to 2 m by 12%.
- The results of the calculation of landslide mass block volumes from raster models indicate that the change in the spatial resolution of the raster cell does not significantly affect the size of the estimated volume. In our research area, the differences in determined volumes between raster models for different LoSRs (0.1 m, 0.25 m, 0.5 m, 1 m, and 2 m) at both time points (2016 and 2020) were at the level of $\pm 1\%$. Thus, there was no dependence on the decrease in the LoSR for the estimation of volumes, which corresponds to the results of the works of Štroner et al. (2019) and Woolard and Colby (2002).
- On the contrary, when determining the volume of the landslide mass block from the 3D mesh data structure, we can state that there is a dependence between the LoSR of the models and the value of the estimated volumes. Thus, the lower the LoSR of 3D mesh models, the greater the difference in estimated volume values is. In our research area, in the case of 3D mesh models, we achieved a difference in the estimated volumes of the landslide mass block between the highest (0.1 m) and the lowest (2 m) LoSR at the level of approximately 6%.
- The character of terrain features also affects the estimation of the volume of the landslide mass block. In the case of territories where there are numerous landforms such as steep slopes (inclination greater than 90°) or overhangs, where locally there is a significant change in elevation values, the influence of spatial resolution is more pronounced. Moreover, even at a high LoSR (0.1 m), there are larger differences between the estimated volumes calculated from the raster and 3D mesh models. In our case, we achieved a difference of more than 2%.

The following conclusions result from the above observations:

- Raster data models slightly overestimate the volume estimate, but the influence of spatial resolution is not significantly manifested. Thus, the spatial resolution of raster models (up to the level of 1 m) does not have a significant effect on volume estimation.
- 3D mesh models with a high spatial resolution (up to 0.25 m) can record the geometry of terrain forms in detail, more precisely determining the course of the surface of the investigated area in three-dimensional space and thus determining its area, resulting in a more accurate estimate of the volume.
- Up to the LoSR \leq 0.5 m (i.e., 0.1 m, 0.25 m, 0.5 m) in the case of calculating volume changes (volume change over a certain period), raster and 3D mesh data models provide a similar result. Even in this case, it appears that raster models slightly overestimate the volume. Above the LoSR \geq 1 m, the results of volume changes in the case of 3D mesh models are already affected by a large degree of surface smoothing, therefore they are unsuitable for evaluating volume changes.

Funding

This work was financially supported by the Slovak Research and Development Agency within the project APVV -22-0024 Physical geomorphometry for physical geographical research and APVV -23-0265 3D technology and machine learning methods for remote environmental monitoring and assessment of river health and also by the grant of the Ministry of Education, Science, Research and Sport of the Slovak Republic within the project VEGA 2/0016/24 Assessment of human impact and climate change to the transformation of river channels using novel 3D geodata, VEGA 1/0780/24 Combining lidar and hyperspectral data with machine learning methods to improve land cover classification and VEGA 1/0085/23 Modeling urban heat islands using geospatial tools.

Author contributions

Ján Šašák: Conceptualization, Methodology, Formal analysis, Writing – Original Draft, Visualization, Resources. Ján Kaňuk: Conceptualization, Formal analysis, Writing – Original Draft, Supervision. Miloš Rusnák: Writing – Original Draft. Jozef Šupinský: Formal analysis, Investigation, Resources.

Disclosure statement

The authors declare that they have no known competing financial interests or personal relationships that could have appeared to influence the work reported in this paper.

References

- Abellán, A., Vilaplana, J. M., Calvet, J., García-Sellés, D., & Asensio, E. (2011). Rockfall monitoring by Terrestrial Laser Scanning – case study of the basaltic rock face at Castellfollit de la Roca (Catalonia, Spain). *Natural Hazards and Earth System Sciences*, 11(3), 829–841. <https://doi.org/10.5194/nhess-11-829-2011>
- Agüera-Vega, F., Agüera-Puntas, M., Martínez-Carricondo, P., Mancini, F., & Carvajal, F. (2020). Effects of point cloud density, interpolation method and grid size on derived Digital Terrain Model accuracy at micro topography level. *International Journal of Remote Sensing*, 41(21), 8281–8299. <https://doi.org/10.1080/01431161.2020.1771788>
- Ai, B., Wang, L., Yang, F., Bu, X., Lin, Y., & Lv, G. (2019). Continuous-scale 3D terrain visualization based on a detail-increment model. *ISPRS International Journal of Geo-Information*, 8(10), Article 465. <https://doi.org/10.3390/ijgi8100465>
- Akay, S. S., Özcan, O., & Şanlı, F. B. (2022). Quantification and visualization of flood-induced morphological changes in meander structures by UAV-based monitoring. *Engineering Science and Technology, an International Journal*, 27, Article 101016. <https://doi.org/10.1016/j.jestch.2021.05.020>
- Alfredsen, K., Haas, C., Tuhtan, J. A., & Zinke, P. (2018). Brief communication: Mapping river ice using drones and structure from motion. *The Cryosphere*, 12(2), 627–633. <https://doi.org/10.5194/tc-12-627-2018>
- Alvarez-Vanhard, E., Corpetti, T., & Houet, T. (2021). UAV & satellite synergies for optical remote sensing applications: A literature review. *Science of Remote Sensing*, 3, Article 100019. <https://doi.org/10.1016/j.srs.2021.100019>
- Antoine, R., Lopez, T., Tanguy, M., Lissak, C., Gailler, L., Labazuy, P., & Fauchard, C. (2020). Geoscientists in the sky: Unmanned aerial vehicles responding to geohazards. *Surveys in Geophysics*, 41(6), 1285–1321. <https://doi.org/10.1007/s10712-020-09611-7>
- ArcGIS Pro. (2023). *ESRI ArcGIS Pro* (Version 3.1.0). <https://www.esri.com/en-us/arcgis/products/arcgis-pro/overview>
- Barnhart, T. B., & Crosby, B. T. (2013). Comparing two methods of surface change detection on an evolving thermokarst using high-temporal-frequency terrestrial laser scanning, Selawik River, Alaska. *Remote Sensing*, 5(6), 2813–2837. <https://doi.org/10.3390/rs5062813>
- Blender. (2018). *3D modelling and rendering package*. Stichting Blender Foundation, Amsterdam. <http://www.blender.org>
- Calle, M., Alho, P., & Benito, G. (2018). Monitoring ephemeral river changes during floods with SfM photogrammetry. *Journal of Iberian Geology*, 44(3), 355–373. <https://doi.org/10.1007/s41513-018-0078-y>
- Caputo, T., Marino, E., Matano, F., Somma, R., Troise, C., & De Natale, G. (2018). Terrestrial Laser Scanning (TLS) data for the analysis of coastal tuff cliff retreat: Application to Coroglio cliff, Naples, Italy. *Annals of Geophysics*, 61(1), 1–18. <https://doi.org/10.4401/ag-7494>
- Casagli, N., Frodella, W., Morelli, S., Tofani, V., Ciampalini, A., Intriari, E., Raspini, F., Rossi, G., Tanteri, L., & Lu, P. (2017). Spaceborne, UAV and ground-based remote sensing techniques for landslide mapping, monitoring and early warning. *Geoenvironmental Disasters*, 4(9), 1–23. <https://doi.org/10.1186/s40677-017-0073-1>
- Chen, Z., Ledoux, H., Khademi, S., & Nan, L. (2022). Reconstructing compact building models from point clouds using deep implicit fields. *ISPRS Journal of Photogrammetry and Remote Sensing*, 194, 58–73. <https://doi.org/10.1016/j.isprsjprs.2022.09.017>

- Cignoni, P., Callieri, M., Corsini, M., Dellepiane, M., Gianovelli, F., & Ranzuglia, G. (2008). MeshLab: An open-source mesh processing tool. In *Eurographics Italian Chapter Conference* (pp. 129–136). The Eurographics Association. <https://diglib.org/bitstream/handle/10.2312/LocalChapterEvents.ItalChap.ItalianChapConf2008.129-136/129-136.pdf?sequence=1&isAllowed=y>
- CloudCompare. (2022). *CloudCompare* (Version 2.12.4) [GPL software]. <http://www.cloudcompare.org/>
- De Sanjosé Blasco, J. J., Serrano-Cañadas, E., Sánchez-Fernández, M., Gómez-Lende, M., & Redweik, P. (2020). Application of multiple geomatic techniques for coastline retreat analysis: The case of Gerra Beach (Cantabrian Coast, Spain). *Remote Sensing*, 12(21), Article 3669. <https://doi.org/10.3390/rs12213669>
- Devoto, S., Macovaz, V., Mantovani, M., Soldati, M., & Furlani, S. (2020). Advantages of using UAV digital photogrammetry in the study of slow-moving coastal landslides. *Remote Sensing*, 12(21), Article 3566. <https://doi.org/10.3390/rs12213566>
- Dolejš, M., Pacina, J., Veselý, M., & Brétt, D. (2020). Aerial bombing crater identification: Exploitation of precise digital terrain models. *ISPRS International Journal of Geo-Information*, 9(12), Article 713. <https://doi.org/10.3390/ijgi9120713>
- Dong, Z., Liang, F., Yang, B., Xu, Y., Zang, Y., Li, J., Wang, Y., Dai, W., Fan, H., Hyyppä, J., & Stilla, U. (2020). Registration of large-scale terrestrial laser scanner point clouds: A review and benchmark. *ISPRS Journal of Photogrammetry and Remote Sensing*, 163, 327–342. <https://doi.org/10.1016/j.isprsjprs.2020.03.013>
- Duró, G., Crosato, A., Kleinhans, M. G., & Uijtewaal, W. S. (2018). Bank erosion processes measured with UAV-SfM along complex banklines of a straight mid-sized river reach. *Earth Surface Dynamics*, 6(4), 933–953. <https://doi.org/10.5194/esurf-6-933-2018>
- Florinsky, I. V., & Pankratov, A. N. (2016). A universal analytical method for digital terrain modeling. *International Journal of Geographical Information Science*, 30(12), 2506–2528. <https://doi.org/10.1080/13658816.2016.1188932>
- Gallay, M., Kaňuk, J., Hochmuth, Z., Meneely, J. D., Hofierka, J., & Sedlák, V. (2015). Large-scale and high-resolution 3-D cave mapping by terrestrial laser scanning: A case study of the Domica Cave, Slovakia. *International Journal of Speleology*, 44(3), 277–291. <https://doi.org/10.5038/1827-806X.44.3.6>
- Gallay, M., Kaňuk, J., Šašak, J., Šupinský, J., Hofierka, J., & Minár, J. (2018). High-resolution digital terrain modelling of a rugged alpine terrain by fusing data from terrestrial laser scanning and UAV photogrammetry. *PeerJ Preprints*, 1–5. <https://doi.org/10.7287/peerj.preprints.27078v1>
- Girardeau-Montaut, D., Roux, M., Marc, R., & Thibault, G. (2005). Change detection on point cloud data acquired with a ground laser scanner. In G. Vosselman & C. Brenner (Eds.), *Proceedings of the ISPRS Workshop Laser Scanning* (pp. 30–35), Enschede, the Netherlands. <https://www.isprs.org/proceedings/xxxvi/3-w19/>
- GRASS GIS. (2022). *GRASS GIS* (Version 7.8.7). <https://grass.osgeo.org/>
- Guerra-Hernández, J., Cosenza, D. N., Rodriguez, L. C. E., Silva, M., Tomé, M., Díaz-Varela, R. A., & González-Ferreiro, E. (2018). Comparison of ALS-and UAV (SfM)-derived high-density point clouds for individual tree detection in Eucalyptus plantations. *International Journal of Remote Sensing*, 39(15–16), 5211–5235. <https://doi.org/10.1080/01431161.2018.1486519>
- Harding, C., Hasiuk, F., & Wood, A. (2021). TouchTerrain—3D printable terrain models. *ISPRS International Journal of Geo-Information*, 10(3), Article 108. <https://doi.org/10.3390/ijgi10030108>
- Hengl, T. (2006). Finding the right pixel size. *Computers & Geosciences*, 32(9), 1283–1298. <https://doi.org/10.1016/j.cageo.2005.11.008>
- Huang, R., Jiang, L., Wang, H., & Yang, B. (2019). A bidirectional analysis method for extracting glacier crevasses from airborne LiDAR point clouds. *Remote Sensing*, 11(20), Article 2373. <https://doi.org/10.3390/rs11202373>
- James, M. R., & Robson, S. (2012). Straightforward reconstruction of 3D surfaces and topography with a camera: Accuracy and geoscience application. *Journal of Geophysical Research: Earth Surface*, 117(F3), Article F030173. <https://doi.org/10.1029/2011JF002289>
- Jiang, N., Li, H., Hu, Y., Zhang, J., Dai, W., Li, C., & Zhou, J. W. (2021). A monitoring method integrating terrestrial laser scanning and unmanned aerial vehicles for different landslide deformation patterns. *IEEE Journal of Selected Topics in Applied Earth Observations and Remote Sensing*, 14, 10242–10255. <https://doi.org/10.1109/JSTARS.2021.3117946>
- Kazhdan, M., Bolitho, M., & Hoppe, H. (2006). *Poisson surface reconstruction*. In K. Polthier & A. Sheffer (Eds.), *Eurographics Symposium on Geometry Processing* (pp. 1–10). The Eurographics Association. <https://hhoppe.com/poissonrecon.pdf>
- Kermarrec, G., Yang, Z., & Czerwonka-Schröder, D. (2022). Classification of terrestrial laser scanner point clouds: A comparison of methods for landslide monitoring from mathematical surface approximation. *Remote Sensing*, 14(20), Article 5099. <https://doi.org/10.3390/rs14205099>
- Kuželka, K., Slavík, M., & Surový, P. (2020). Very high density point clouds from UAV laser scanning for automatic tree stem detection and direct diameter measurement. *Remote Sensing*, 12(8), Article 1236. <https://doi.org/10.3390/rs12081236>
- Kyriou, A., Nikolakopoulos, K., Koukouvelas, I., & Lampropoulou, P. (2021). Repeated UAV campaigns, GNSS measurements, GIS, and petrographic analyses for landslide mapping and monitoring. *Minerals*, 11(3), Article 300. <https://doi.org/10.3390/min11030300>
- Lague, D., Brodu, N., & Leroux, J. (2013). Accurate 3D comparison of complex topography with terrestrial laser scanner: Application to the Rangitikei canyon (NZ). *ISPRS Journal of Photogrammetry and Remote Sensing*, 82, 10–26. <https://doi.org/10.1016/j.isprsjprs.2013.04.009>
- LAStools. (2023). *Efficient LiDAR processing software* (Version 220926, academic). <https://rapidlasso.de/lastools-220107/>
- Lissak, C., Bartsch, A., De Michele, M., Gomez, C., Maquaire, O., Raucoules, D., & Roulland, T. (2020). Remote sensing for assessing landslides and associated hazards. *Surveys in Geophysics*, 41(6), 1391–1435. <https://doi.org/10.1007/s10712-020-09609-1>
- Mancini, F., Castagnetti, C., Rossi, P., Dubbini, M., Fazio, N. L., Perroti, M., & Lollino, P. (2017). An integrated procedure to assess the stability of coastal rocky cliffs: From UAV close-range photogrammetry to geomechanical finite element modeling. *Remote Sensing*, 9(12), Article 1235. <https://doi.org/10.3390/rs9121235>
- Marotta, F., Teruggi, S., Achille, C., Vassena, G. P. M., & Fassi, F. (2021). Integrated laser scanner techniques to produce high-resolution DTM of vegetated territory. *Remote Sensing*, 13(13), Article 2504. <https://doi.org/10.3390/rs13132504>
- Mazzanti, P., Caporossi, P., Brunetti, A., Mohammadi, F. I., & Bozzano, F. (2021). Short-term geomorphological evolution of the Poggio Baldi landslide upper scarp via 3D change detection. *Landslides*, 18(7), 2367–2381. <https://doi.org/10.1007/s10346-021-01647-z>
- Meng, Q., Li, W., Raspini, F., Xu, Q., Peng, Y., Ju, Y., Zheng, Y., & Casagli, N. (2021). Time-series analysis of the evolution of large-scale loess landslides using InSAR and UAV photogram-

- metry techniques: A case study in Hongheyan, Gansu Province, Northwest China. *Landslides*, 18(1), 251–265. <https://doi.org/10.1007/s10346-020-01490-8>
- Mineo, S., Caliò, D., & Pappalardo, G. (2022). UAV-based photogrammetry and infrared thermography applied to rock mass survey for geomechanical purposes. *Remote Sensing*, 14(3), Article 473. <https://doi.org/10.3390/rs14030473>
- Mirtich, B. (1996). Fast and accurate computation of polyhedral mass properties. *Journal of Graphics Tools*, 1(2), 31–50. <https://doi.org/10.1080/10867651.1996.10487458>
- Mishra, N., Chaudhuri, G., Mainali, K., Mal, S., Tiruwa, B., & Singh, P. (2020). Quantifying melt dynamics on a debris-covered Himalayan glacier using repeated UAS photogrammetry derived DSM and point cloud differencing. Preprints. <https://doi.org/10.20944/preprints202007.0555.v1>
- Mitášová, H., & Mitáš, L. (1993). Interpolation by regularized spline with tension: I. Theory and implementation. *Mathematical Geology*, 25, 641–655. <https://doi.org/10.1007/BF00893171>
- Mitasova, H., Hardin, E., Overton, M., & Harmon, R. S. (2009). New spatial measures of terrain dynamics derived from time series of lidar data. In *2009 17th International Conference on Geoinformatics* (pp. 1–6), Fairfax, VA, USA. <https://doi.org/10.1109/GEOINFORMATICS.2009.5293539>
- Mucherino, A., Papajorgji, P. J., & Pardalos, P. M. (2009). k-nearest neighbor classification. In *Springer optimization and its applications: Vol. 34. Data mining in agriculture* (pp. 83–106). Springer. https://doi.org/10.1007/978-0-387-88615-2_4
- Münzinger, M., Prechtel, N., & Behnisch, M. (2022). Mapping the urban forest in detail: From LiDAR point clouds to 3D tree models. *Urban Forestry & Urban Greening*, 74, Article 127637. <https://doi.org/10.1016/j.ufug.2022.127637>
- Nemčok, J., Bezák, V., Biely, A., Gorek, A., Gross, P., Halouzka, R., Janák, M., Kahan, Š., Mello, J., Reichwalder, P., Rackowski, W., Roniewicz, P., Ryka, W., Wiczorek, J., & Zelman, J. (1994). *Geologická mapa Tatier v mierke 1:50 000*. Geologický ústav Dionýza Štúra. <https://www.geology.sk/24-geologicka-mapatatier-1-50-000/>
- Nguyen, V. T., Fournier, R. A., Côté, J. F., & Pimont, F. (2022). Estimation of vertical plant area density from single return terrestrial laser scanning point clouds acquired in forest environments. *Remote Sensing of Environment*, 279, Article 113115. <https://doi.org/10.1016/j.rse.2022.113115>
- Nourbakhshbeidokhti, S., Kinoshita, A. M., Chin, A., & Florshheim, J. L. (2019). A workflow to estimate topographic and volumetric changes and errors in channel sedimentation after disturbance. *Remote Sensing*, 11(5), Article 586. <https://doi.org/10.3390/rs11050586>
- Pellicani, R., Argentiero, I., Manzari, P., Spilotro, G., Marzo, C., Ermini, R., & Apollonio, C. (2019). UAV and airborne LiDAR data for interpreting kinematic evolution of landslide movements: The case study of the Montescaglioso landslide (Southern Italy). *Geosciences*, 9(6), Article 248. <https://doi.org/10.3390/geosciences9060248>
- Peterson, S., Lopez, J., & Munjy, R. (2019). Comparison of UAV imagery-derived point cloud to terrestrial laser scanner point cloud. *ISPRS Annals of the Photogrammetry, Remote Sensing and Spatial Information Sciences*, 4, 149–155. <https://doi.org/10.5194/isprs-annals-IV-2-W5-149-2019>
- Peytavie, A., Galin, E., Grosjean, J., & Merillou, S. (2009). Arches: A framework for modeling complex terrains. *Computer Graphics Forum*, 28(2), 457–467. <https://doi.org/10.1111/j.1467-8659.2009.01385.x>
- Rice, A. R., Cassidy, R., Jordan, P., Rogers, D., & Arnscheidt, J. (2021). Fine-scale quantification of stream bank geomorphic volume loss caused by cattle access. *Science of the Total Environment*, 769, Article 144468. <https://doi.org/10.1016/j.scitotenv.2020.144468>
- Roulland, T., Maquaire, O., Costa, S., Medjkane, M., Davidson, R., Fauchard, C., & Antoine, R. (2022). Seasonal activity quantification of coast badlands by TLS monitoring over five years at the “Vaches Noires” cliffs (Normandy, France). *Geomorphology*, 400, Article 108083. <https://doi.org/10.1016/j.geomorph.2021.108083>
- Rusnák, M., Kaňuk, J., Kidová, A., Šašak, J., Lehotský, M., Pöpl, R., & Šupinský, J. (2020). Channel and cut-bluff failure connectivity in a river system: Case study of the braided-wandering Belá River, Western Carpathians, Slovakia. *Science of the Total Environment*, 733, Article 139409. <https://doi.org/10.1016/j.scitotenv.2020.139409>
- Sailer, R., Bollmann, E., Hoinkes, S., Rieg, L., Sproß, M., & Stötter, J. (2012). Quantification of geomorphodynamics in glaciated and recently deglaciated terrain based on airborne laser scanning data. *Geografiska Annaler, Series A: Physical Geography*, 94, 17–32. <https://doi.org/10.1111/j.1468-0459.2012.00456.x>
- Scaioni, M., Feng, T., Lu, P., Qiao, G., Tong, X., Li, R., Barazzetti, L., Previtali, M., & Roncella, R. (2015). Close-range photogrammetric techniques for deformation measurement: Applications to landslides. In M. Scaioni (Ed.), *Modern technologies for landslide monitoring and prediction* (pp. 13–41). Springer Natural Hazards. https://doi.org/10.1007/978-3-662-45931-7_2
- Stumvoll, M. J., Schmaltz, E. M., & Glade, T. (2021). Dynamic characterization of a slow-moving landslide system—Assessing the challenges of small process scales utilizing multi-temporal TLS data. *Geomorphology*, 389, Article 107803. <https://doi.org/10.1016/j.geomorph.2021.107803>
- Šašak, J., Gallay, M., Kaňuk, J., Hofierka, J., & Minár, J. (2019). Combined use of terrestrial laser scanning and UAV photogrammetry in mapping alpine terrain. *Remote Sensing*, 11(18), Article 2154. <https://doi.org/10.3390/rs11182154>
- Šupinský, J., Kaňuk, J., Hochmuth, Z., & Gallay, M. (2019). Detecting dynamics of cave floor ice with selective cloud-to-cloud approach. *The Cryosphere*, 13(11), 2835–2851. <https://doi.org/10.5194/tc-13-2835-2019>
- Štroner, M., Křemen, T., Braun, J., Urban, R., Blistan, P., & Kovanič, L. (2019). Comparison of 2.5D volume calculation methods and software solutions using point clouds scanned before and after mining. *Acta Montanistica Slovaca*, 24(4), 296–306. <https://actamont.tuke.sk/pdf/2019/n4/2stroner.pdf>
- Tian, J., Dai, T., Li, H., Liao, C., Teng, W., Hu, Q., Ma, W., & Xu, Y. (2019). A novel tree height extraction approach for individual trees by combining TLS and UAV image-based point cloud integration. *Forests*, 10(7), Article 537. <https://doi.org/10.3390/f10070537>
- Wade, T. G., Wickham, J. D., Nash, M. S., Neale, A. C., Riitters, K. H., & Jones, K. B. (2003). A comparison of vector and raster GIS methods for calculating landscape metrics used in environmental assessments. *Photogrammetric Engineering & Remote Sensing*, 69(12), 1399–1405. <https://doi.org/10.14358/PERS.69.12.1399>
- Wang, Q., & Kim, M. K. (2019). Applications of 3D point cloud data in the construction industry: A fifteen-year review from 2004 to 2018. *Advanced Engineering Informatics*, 39, 306–319. <https://doi.org/10.1016/j.aei.2019.02.007>
- Williams, R. (2012). DEMs of difference. *Geomorphological Techniques*, 2, 1–17. https://www.researchgate.net/publication/310596075_DEMs_of_Difference/citations
- Woolard, J. W., & Colby, J. D. (2002). Spatial characterization, resolution, and volumetric change of coastal dunes using airborne

- LIDAR: Cape Hatteras, North Carolina. *Geomorphology*, 48(1–3), 269–287. [https://doi.org/10.1016/S0169-555X\(02\)00185-X](https://doi.org/10.1016/S0169-555X(02)00185-X)
- Zhang, H., Bauters, M., Boeckx, P., & Van Oost, K. (2021). Mapping canopy heights in dense tropical forests using low-cost UAV-derived photogrammetric point clouds and machine learning approaches. *Remote Sensing*, 13(18), Article 3777. <https://doi.org/10.3390/rs13183777>
- Zhang, Y., Shen, C., Zhou, S., & Luo, X. (2022). Analysis of the influence of forests on landslides in the Bijie Area of Guizhou. *Forests*, 13(7), Article 1136. <https://doi.org/10.3390/f13071136>
- Zhang, Z., Gerke, M., Vosselman, G., & Yang, M. Y. (2018). Filtering photogrammetric point clouds using standard LiDAR filters towards DTM generation. *ISPRS Annals of the Photogrammetry, Remote Sensing & Spatial Information Sciences*, 4(2), 319–326. <https://doi.org/10.5194/isprs-annals-IV-2-319-2018>
- Zhong, C., Liu, Y., Gao, P., Chen, W., Li, H., Hou, Y., Nuremanguli, T., & Ma, H. (2019). Landslide mapping with remote sensing: Challenges and opportunities. *International Journal of Remote Sensing*, 41(4), 1555–1581. <https://doi.org/10.1080/01431161.2019.1672904>
- Zhou, Q., Grinspun, E., Zorin, D., & Jacobson, A. (2016). Mesh arrangements for solid geometry. *ACM Transactions on Graphics*, 35(4), 1–15. <https://doi.org/10.1145/2897824.2925901>